FOAM3D: A Numerical Simulator for Mechanistic Prediction of Foam Displacement in Multidimensions

A. R. Kovscek[1], T. W. Patzek[1,2], and C. J. Radke[1,3]

[1] Earth Sciences Division, Lawrence Berkeley Laboratory,
[2] Dept. of Materials Science and Mineral Engineering
[3] Dept. of Chemical Engineering
University of California, Berkeley, CA 94720

INTRODUCTION

Field application of foam is a technically viable enhanced oil recovery process (EOR) as demonstrated by recent steam-foam field studies [1,2]. Traditional gas-displacement processes, such as steam drive, are improved substantially by controlling gas mobility and thereby improving volumetric displacement efficiency. For instance, Patzek and Koinis [2] showed major oil-recovery response after about two years of foam injection in two different pilot studies at the Kern River field. They report increased production of 5.5 to 14% of the original oil in place over a five year period.

Because reservoir-scale simulation is a vital component of the engineering and economic evaluation of any EOR project, efficient application of foam as a displacement fluid requires a predictive numerical model of foam displacement. A mechanistic model would also expedite scale-up of the process from the laboratory to the field scale. No general, mechanistic, field-scale model for foam displacement is currently in use.

The population balance method for modeling foam in porous media [3] is mechanistic and incorporates foam into reservoir simulators in a manner that is analogous to energy and species mass balances. Accordingly, a separate conservation equation is written for the concentration of foam bubbles (i.e., texture). This simply adds another component to a standard compositional simulator.

This paper extends our one-dimensional foam displacement model [4,5] to multidimensional, compositional reservoir simulation. We have incorporated a conservation equation for the number density of foam bubbles into M2NOTS [6], a variant of TOUGH2. The foam conservation equation is treated with a fully implicit, backward differencing scheme, in analogy to the other component mass balances. The simulator employs saturation and surfactant-concentration-dependent rate expressions for lamella formation and destruction. Lamella mobilization is similarly included. To allow direct comparison with our previous one-dimensional results [4,5] , we discuss only isothermal and oil-free systems.

Foam in Porous Media

Foam microstructure in porous media is unique [7] and determines gas mobility within porous media. Accordingly, to model gas mobility it is important to understand foamed-gas microstructure. In water-wet porous media, the wetting surfactant solution remains continuous, fills the smallest pore spaces, coats pore walls in gas-occupied regions. Gas bubbles flow through the largest, least resistive pore space while significant bubble trapping occurs in the intermediate-sized pore channels where the local pressure gradient is insufficient to mobilize lamellae.

Foam reduces gas mobility in two manners. First, stationary or trapped foam blocks a large number of channels that otherwise carry gas. Gas tracer studies [8] show that the fraction of gas trapped within a foam at steady state in sandstones is quite large and lies between 85 and 99%. Second, bubble trains within the flowing fraction encounter significant drag because of the presence of pore walls and constrictions, and because the gas/liquid interfacial area of a flowing bubble is constantly altered by viscous and capillary forces. Hence, foam mobility depends strongly on the fraction of gas trapped and on the texture or number density of foam bubbles.

Bubble trains are in a constant state of rearrangement by varied foam generation and destruction mechanisms [7]. Individual foam bubbles are molded and shaped by pore-level making and breaking processes that depend strongly on the porous medium. More detailed summaries of the pore-level distribution of foam and of the mechanisms controlling texture are given in refs. [4] and [7].

FOAM DISPLACEMENT MODEL

The power of the population balance method lies in addressing directly the evolution of foam texture and, in turn, reductions in gas mobility. Gas mobility is assessed from the concentration of bubbles. Further, the method is mechanistic in that well-documented pore-level events are portrayed in foam generation, coalescence, and constitutive relations. Most importantly, the population balance method provides a general framework where all the relevant physics of foam generation and transport may be expressed. Only a brief summary of the method is given here as considerable details are available in the literature [4,5].

The requisite material balance equations for chemical species i during multiphase flow in porous media are written

$$\frac{\partial}{\partial t}\left[\phi\sum_j (S_j C_{i,j} + \Gamma_{i,j})\right] + \sum_j \nabla\bullet\vec{F}_{i,j} = \sum_j q_{i,j} \quad (1)$$

where S is the saturation of phase j, C is the molar concentration of species i in phase j, Γ is the absorption or partitioning losses of species i from phase j in units of moles per void volume, $\vec{F}$ is the vector of convective plus diffusive flux of species i in phase j, and q is a rate of generation of i in phase j per unit volume of porous medium. To obtain the total mass of species i, we sum over all phases j.

In the foam bubble population balance, $S_f n_f$ replaces $S_i C_{i,j}$ where n_f is the number concentration or number density of foam bubbles per unit volume of flowing gas, and S_f is the saturation of flowing gas. Hence, the first term of the time derivative is the rate at which flowing foam texture becomes finer or coarser per unit rock volume. Since foam partitions into flowing and stationary portions, Γ becomes $S_t n_t$ where S_t and n_t are the saturation of the stationary gas and the texture of the trapped foam per unit volume of trapped gas, respectively. Thus, the second term of the time derivative gives the net rate at which bubbles trap. Trapped and flowing foam saturation sum to the overall gas saturation, $S_g = S_f + S_g$. The second term on the left of Eq. (1) tracks the convection of foam bubbles where the flux, $\vec{F}$, is given by $\vec{u}_f n_f$, and $\vec{u}_f$ is the Darcy velocity of the flowing foam. Finally, q becomes the net rate of generation of foam bubbles. Because foam is present only in the gas phase, there is no need to sum over all phases. Within the above framework, foam is a component of the gas phase, and the physics of foam generation and transport become amenable to standard reservoir simulation practice.

The net rate of foam generation:

$$q_f = \phi S_g\left[k_1|\vec{v}_w||\vec{v}_f|^{1/3} - k_{-1}(P_c)|\vec{v}_f n_f|\right] \quad (2)$$

is written per unit volume of gas. In the simulations to follow, we do not inject pregenerated foam, and so, we do not require a source/sink term for bubbles. Interstitial velocities, *i.e.*, $\vec{v}_i = \vec{u}_i/\phi S_i$, are local vector quantities that depend on the local saturation and total potential gradient, including gravity and capillary pressure. Foam generation arises from snap-off of gas, and is expressed as a power-law relationship that is proportional to the magnitude of the flux of surfactant solution multiplied by the 1/3 power of the magnitude of the interstitial gas velocity [9]. The liquid-velocity dependence originates from the net imposed liquid flow through pores occupied by both gas and liquid, while the gas-velocity dependence arises from the time for a newly formed lens to exit a pore [9]. Snap-off is sensibly independent of surfactant properties consistent with its mechanical origin [7].

To prevent coalescence of newly formed gas bubbles, a surfactant must stabilize the thin-liquid films. Foam lamellae form given sufficient suction capillary pressure and a stabilizing surfactant. However, too high a suction-capillary pressure will collapse a lamella [7]. A flowing lamella is vulnerable to breakage in termination sites as it flows into a divergent pore space where it is stretched rapidly. If sufficient time does not elapse for surfactant solution to flow into a stretched lamella and heal it, coalescence ensues.

Equation (2) shows that foam lamellae are destroyed in proportion to the magnitude of their interstitial flux, $\vec{v}_f n_f$, into such termination sites. The coalescence rate constant, $k_{-1}(P_c)$, varies strongly with the local capillary pressure and surfactant formulation. It is given by

$$k_{-1}(P_c) = k^o_{-1}\left(\frac{P_c}{P_c^* - P_c}\right)^2, \quad (3),$$

where the scaling factor, k^o_{-1}, is taken as a constant and P_c^* is the limiting capillary pressure for foam coalescence [10].

The "limiting capillary pressure," P_c^*, as identified by Khatib *et al* [10] refers to the characteristic value of capillary pressure that a porous medium approaches during strong foam flow and is set primarily by surfactant formulation and concentration. Highly concentrated foamer solutions and robust surfactants lead to high a P_c^*. Equation (3) correctly predicts that at high capillary pressures or for ineffective foamer solutions, k_{-1} is quite high [10]. The foam coalescence rate approaches infinity as the porous medium capillary pressure approaches P_c^*.

In addition to bubble kinetic expressions, the mass balance statements for chemical species demand constitutive relationships for the convection of foam and wetting liquid phases. Darcy's law is retained, including standard multiphase relative permeability functions. However, for flowing foam, we replace the gas viscosity with an effective viscosity relation for foam. Since flowing gas bubbles deposit and slide over thin lubricating films of wetting liquid on pore walls, they do not exhibit a Newtonian viscosity. We adopt an effective viscosity relation that increases foam effective viscosity as texture increases, but is also shear thinning

$$\mu_f = \mu_g + \frac{\alpha n_f}{|\vec{v}_f|^{1/3}}. \quad (4),$$

where α is constant of proportionality dependent mainly upon the surfactant system. In the limit of no flowing foam, we recover the gas viscosity. This relation is consistent with the classical result of Bretherton [11] for slow bubble flow in capillary tubes .

Finally, stationary foam blocks large portions of the cross-sectional area available for gas flow and, thus, must be accounted for to determine gas flux. Since the portion of gas that actually flows partitions selectively into the largest, least resistive flow channels, we adopt a standard Stone-type model [12] for relative permeability that, along with effective viscosity, specifies gas-phase flow resistance. Because wetting aqueous liquid flows in the smallest pore space, its relative permeability is unaffected by the presence of flowing and stationary foam. Since flowing foam partitions selectively into the largest pore space, the relative permeability of the nonwetting flowing gas is a function of only S_f. Consequently, gas mobility is much reduced in comparison to an unfoamed gas propagating through a porous medium, because the fraction of gas flowing at any instant is quite small [8].

FOAM3D

We treat foam bubbles within FOAM3D as an insoluble, chemically inert component of the gas phase. Thus, the additional transport equation for foam bubble texture described above is added to the mass balances for water, gas, and n organic components. The discretized foam bubble equation is fully implicit with upstream weighting of the gas-phase mobility consistent with all other chemical species. In each grid block, the magnitude of the vectors representing the interstitial gas and liquid velocities are used to compute foam generation and coalescence rates from Eq. (2). The magnitude of each velocity is obtained by first summing the flow of each phase into and out of a grid block in the three orthogonal directions. Then the average flow in each direction is taken and the magnitude of the resultant vector used to calculate foam generation and coalescence rates.

Numerical values of the population balance simulation parameters are determined from only steady-state measurements in one-dimensional linear flow. Steady-state flow trends, saturation, and pressure drop profiles are matched. These can all be obtained within one experimental run. The suite of foam displacement parameters are not adjusted to accommodate different types of transient injection or initial conditions. Parameter values used here are taken from refs. [4,5] and apply specifically to very strong foams in the absence of oil.

NUMERICAL MODEL RESULTS

Because there are many initial conditions, types of injection, and multidimensional geometries of interest, we present the results from only two illustrative examples. First, we compare simulator predictions against experimental results for the simultaneous injection of nitrogen and foamer solution into a linear core saturated with surfactant. Second, foam displacement is simulated in a two-dimensional linear layer with gravity. To avoid confusion between foam formation, surfactant propagation and adsorption, foam-oil interaction, and partitioning of surfactant into the oil phase, we choose a porous medium that is fully saturated with surfactant solution as the initial condition. That is, $S_w = 1$, initially and rock adsorption of surfactant is satisfied. Nitrogen and foamer solution are coinjected simultaneously. Thus, we focus attention on foam formation, coalescence, transport, and reduction of gas mobility.

Linear Core

In the first example, nitrogen is injected continuously into a linear core of length 0.60 m at a rate of 0.43 m/day relative to the exit pressure of 4.8 MPa. Foamer solution is also injected continuously at 0.046 m/day to give a quality or gas fractional flow of 0.90 at the core exit. These flow rates and initial conditions correspond exactly to previous experiments conducted in a 1.3-μm^2 Boise sandstone [4,5] with a length of 0.60 m. The foamer was a saline solution (0.83 wt% NaCl) with 0.83 wt% active AOS 1416 (C_{14-16} alpha olefin sulfonate, Bioterg AS-40, Stepan).

Figures 1 and 2 display the transient experimental and simulated saturation and pressure profiles, respectively. Figure 3 displays the foam texture profiles generated by FOAM3D. Simulator results are represented by solid lines. Dashed lines simply connect the individual data points. Elapsed time is given as pore volumes of total fluid injected, that is, as the ratio of total volumetric flow rate at exit conditions multiplied by time and divided by the core void volume.

Steep saturation fronts are measured and predicted at all time levels in Fig. 1 whereby aqueous phase saturation upstream of the front is roughly 30% and downstream it is 100%. Model fronts are somewhat steeper and sharper than those measured experimentally, but the theoretical saturation profiles track experimental results very well. From the saturation profiles, it is apparaent that foam moves through the core in a piston-like fashion. Rapid foam generation and liquid desaturation occur at the core inlet, even though nitrogen and surfactant solution are injected separately. A region of net foam generation near the core inlet is evident in the transient pressure profiles of Fig. 2. Pressure gradients near the inlet are shallow, indicating that flow resistance is small and foam textures are coarse consistent with the injection of unfoamed gas. Figure 3 reports the predicted foam texture as a function of dimensionless distance and time. We find a coarsely textured foam near the inlet, but beyond the first fifth of the core, foam texture becomes very fine and nearly constant at each time level. High pressure gradients and fine foam textures are seen where liquid saturation is low and *vice versa.*

Figure 4 contrasts the highly efficient foam displacement above by displaying a simulated gas displacement. Initially the core is completely filled with aqueous liquid, but no stabilizing surfactant is present.

Whereas foam displacement is characterized by steep, sharp saturation fronts and long times to the first appearance of foam at the core outlet, gas displacement is characterized by the slow displacement of water and the early appearance of gas at the production end of the core. Obviously, foam increases gas displacement efficiency in linear core floods by several orders of magnitude.

Homogeneous Linear Layer with Gravity

The second example is foam generation in a linear, 1.3-μm^2, homogeneous layer where gravitational effects are appreciable. The layer is 0.6 m square with impermeable top and bottom boundaries. The y-axis corresponds to the vertical direction and the scale gives the distance from the origin in meters. Unfoamed gas and surfactant solution are injected in the lower quarter of the left boundary and production occurs at the right boundary against a constant pressure of 4.8 MPa. Injection rates are identical to the previous linear case: 0.43 m/day of gas and 0.046 m/day of foamer solution, where these superficial velocities are taken over the entire vertical interval.

To contrast foamed and unfoamed gas injection, Figure 5 displays the gas saturation contours after 0.10 PV of total injection in the complete absence of surfactant. The gray-scale shading of the figure illustrates the gas saturation. Unshaded portions of the figure refer to a gas saturation of zero and progressively darker shading refers to larger gas saturations. Black shading refers to a gas saturation of one. In Fig. 5, the areas contacted by gas are poorly swept as indicated by their light gray shading. Further, the unfoamed gas is quickly driven toward the top of the layer by buoyancy. A tongue of gas forms along the upper boundary due to gravity override that leaves areas along the lower horizontal boundary unswept by gas.

When surfactant solution initially saturates the homogeneous layer, foam generation is rapid and provides effective control of gravity override, as illustrated in Fig. 6. Figure 6a gives the gas saturation contours at 0.10 PV of total gas and foamer solution injection. This plot is dramatically different from Fig. 5. First, foam propagates spherically. Buoyancy-driven flow of gas upward causes foam generation and an increase in flow resistance that slows upward gas propagation. To balance flow resistance, foam generates almost equally in the horizontal and vertical directions, leading to spherical growth of the foam-filled zone. Additionally, the gas saturations in Figure 6a show that efficient displacement is occurring. The dark, nearly uniform shading of the foam-filled region corresponds to a gas saturation of roughly 0.70. The gas saturation falls off abruptly at the edges of the gas-filled region, indicating a sharp displacement front.

Figures 6b through 6d display the subsequent gas saturation contours at times of 0.20, 0.30, and 0.40 PV, respectively. Spherical growth of the foam zone and efficient displacement continue as illustrated by these figures. Foam, in this example, effectively negates gravity override. When foam reaches the upper boundary of the layer, displacement continues toward the right in the horizontal direction as a piston-like front that expels the surfactant-laden water.

SUMMARY

We have shown that it is possible to model foam displacement mechanistically in multidimensions. Beginning with M2NOTS, an n-component compositional simulator, the foam bubble population balance equations are successfully incorporated within the simulator's fully implicit framework. The mechanistic population balance approach allows us to insert the physics of foam displacement directly into a reservoir simulator. Foam is treated as a insoluble, chemically inert "component" of the gas phase and the evolution of foam texture is modeled explicitly through pore-level foam generation and coalescence equations. As foam mechanisms become better understood, this framework allows for their inclusion.

REFERENCES

1. Friedmann, F., M.E. Smith, W.R. Guice, J.M. Gump, and D.G. Nelson, *Soc. Pet. Eng. Res. Eng*, 9 (1994) 297-304.
2. Patzek, T.W. and M.T. Koinis, *J. Petr. Tech.*, 42 (1990) 496-503.
3. Falls, A.H., G.J. Hirasaki, T.W. Patzek, P.A. Gauglitz, D.D. Miller, and T. Ratulowski, *Soc. Pet. Eng. Res. Eng.*, 3 (1988) 884-892.
4. Kovscek, A.R. and C.J. Radke, in *Foams in the Petroleum Industry*, L.L. Schramm, (Ed.), American Chemical Society, Washington, D.C., 1994, 115-163.
5. Kovscek, A.R., T.W. Patzek, and C.J. Radke , SPE 26402, presented at the the 68th Annual Technical Conference of SPE, Houston, TX, October 1993.
6. Adenekan, A.E., T.W. Patzek, and K. Pruess, *Water Resources Research*, 29 (1993) 3727-3740.
7. Chambers, K.T. and C.J. Radke, in *Interfacial Phenomena in Petroleum Recovery*, N.R. Morrow, (Ed.), Marcel Dekker Inc., New York, 1991, 191-255.
8. Gillis, J.V. and C.J. Radke, SPE 20519, presented at the 65th SPE Annual Technical Conference, New Orleans, LA, September, 1990.
9. Kovscek, A.R., *Foam Displacement in Porous Media: Experiment and Mechanistic Prediction by the Population Balance Method,* Ph.D. Thesis, University of California, Berkeley, 1994.
10. Khatib, Z.I., G.J. Hirasaki, and A.H. Falls, *Soc. Pet. Eng. Res. Eng.*, 3 (1988) 919-926.
11. Bretherton, F.P., *J. Fluid Mech.*, 10 (1961) 166-188.
12. Stone, H.L., *J. Pet. Tech.*, 22 (1970) 214-218.

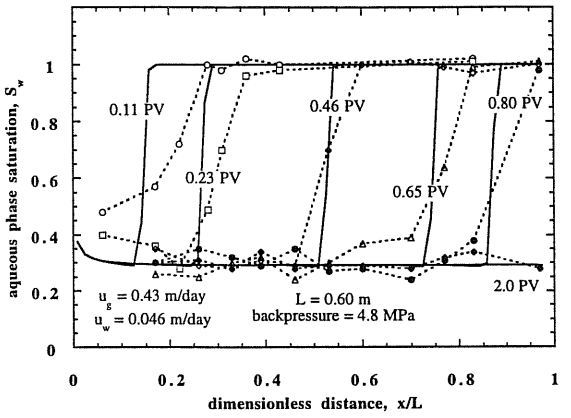

Figure1: Experimental and model transient aqueous-phase saturation profiles for the simultaneous injection of gas and foamer solution at fixed mass rates. The porous medium is presaturated with surfactant solution.

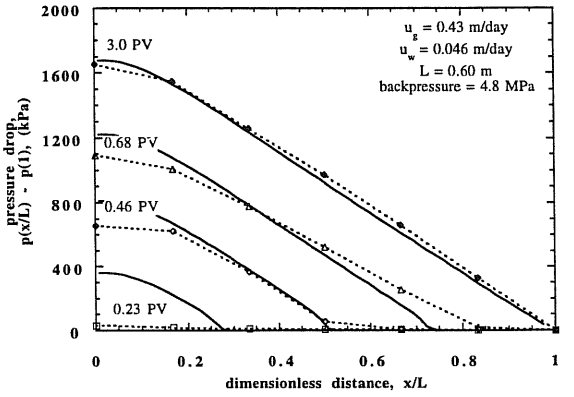

Figure 2: Experimental and model transient pressure profiles for the simultaneous injection of gas and foamer at fixed mass rates. The porous medium is presaturated with surfactant solution.

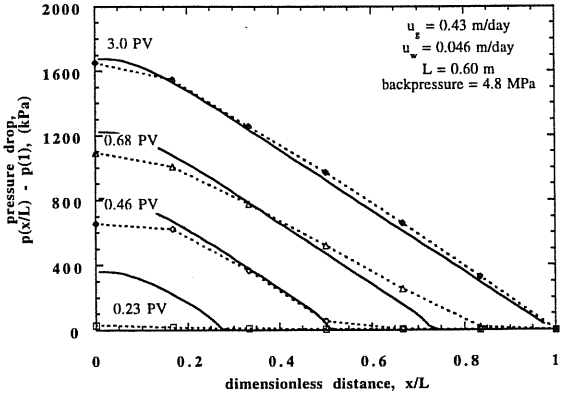

Figure 2: Experimental and model transient pressure profiles for the simultaneous injection of gas and foamer at fixed mass rates. The porous medium is presaturated with surfactant solution.

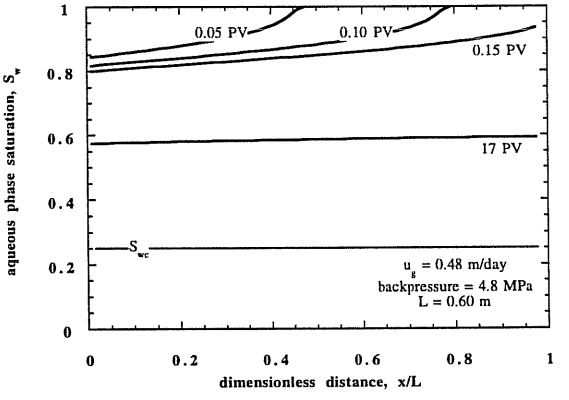

Figure 4: Transient aqueous-phase saturation profiles for the continuous injection of unfoamed gas.

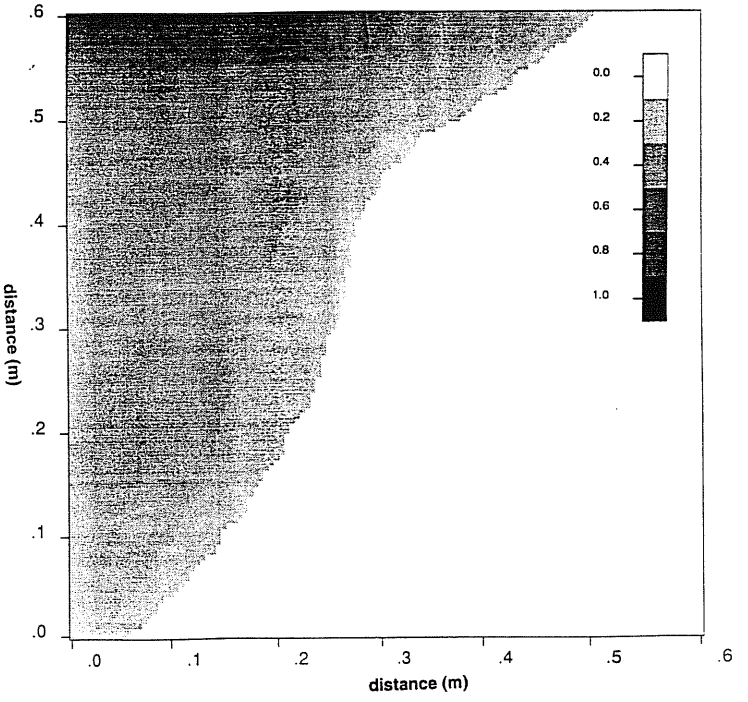

Figure 5: Gas saturation profile after 0.10 PV of unfoamed gas and liquid injection into a homogeneous linear layer.

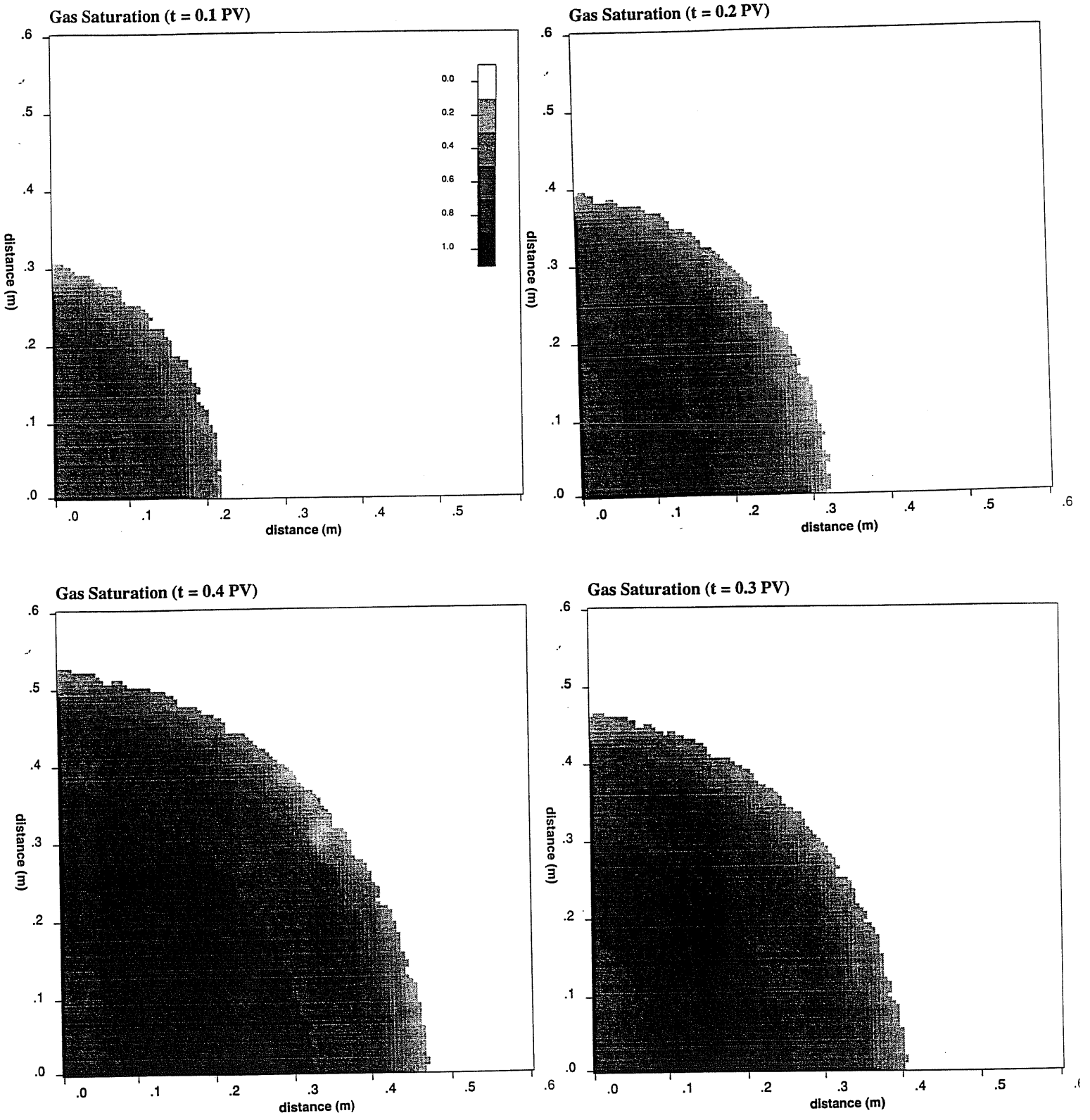

Figure 6: Gas saturation profile after (a) 0.10 PV, (b)0.20 PV, (c) 0.30 PV, and (d) 0.40 PVof foam injection into a homogeneous linear layer.